Morphology and Mechanical Properties of Multiwalled Carbon Nanotubes Reinforced Nylon-6 Composites

Tianxi Liu,*,† In Yee Phang, Lu Shen, Shue Yin Chow, and Wei-De Zhang*

Institute of Materials Research and Engineering, 3 Research Link, Singapore 117602

Received May 3, 2004; Revised Manuscript Received July 16, 2004

ABSTRACT: Multiwalled carbon nanotubes (MWNTs)/nylon-6 (PA6) nanocomposites with different MWNTs loadings have been prepared by the simple melt-compounding approach. A fine and homogeneous dispersion of MWNTs throughout PA6 matrix is observed by transmission electron microscopy. Scanning electron microscopy observation on the fracture surfaces of the composites shows not only a uniform dispersion of MWNTs but also a strong interfacial adhesion with the matrix, as evidenced by the presence of many broken but strongly embedded carbon nanotubes (CNTs) in the matrix and by the absence of debonding of CNTs from the matrix. Beadlike morphology is also observed along the stretched CNTs and their bundles, probably indicating the anchoring locations of the CNTs defects (within the beads) along the tubes where the PA6 matrix has strong interfacial interactions with the CNTs, thus being favorable to stress transfer from polymer to CNTs. Mechanical testing (by tensile and nanoindentation tests as well as dynamic mechanical analysis) shows that, compared with neat PA6, the elastic modulus and the yield strength of the composite are greatly improved by about 214% and 162%, respectively, with incorporating only 2 wt % MWNTs. In addition, a unique crystallization and melting behavior of MWNTs/PA6 composites are observed and discussed by combining differential scanning calorimetry and X-ray diffraction; that is, *only* the α-form crystals are observed in MWNTs/PA6 composites, which is quite different from the case observed in PA6/clay nanocomposites.

Introduction

On the basis of their unique and remarkable mechanical and electrical properties of carbon nanotubes (CNTs), many structural and smart applications of CNTs have been proposed, including quantum wires, tiny electronic devices, heterojunction devices, and electron emitters as well as lighter, smaller, and higher performance structures for aerospace and many other industrial fields.[1,2] Among them, one of the most intriguing applications of CNTs is the polymer/CNTs nanocomposites.[3−14] The combination of high aspect ratio, small size, very low density, and, more importantly, excellent physical properties (such as extremely high mechanical strength and stiffness, high electrical and thermal conductivity) makes CNTs perfect candidates as ideal reinforcing fillers in high strength, lightweight polymer nanocomposites with high performance[9,15,16] and multifunctions.[17−21] However, the challenges for developing high performance CNTs/polymer nanocomposites are (i) homogeneous *dispersion* of CNTs in the polymeric matrix and (ii) strong interfacial interactions so as to effect efficient *load transfer* from the polymeric matrix to the CNTs. Without chemically bonding, load transfer between the CNTs and the matrix (i.e., across the CNTs/polymer interfaces due to the chemically smooth CNTs surfaces) mainly comes from electrostatic and van der Waals interactions.[22] Much efficiency of load transfer can be realized by chemical bonding of polymeric matrix with functionalized CNTs.[23,24]

Despite advantages of single-walled carbon nanotubes (SWNTs) compared with multiwalled ones (MWNTs), a problem associated with the fabrication of polymer composites using SWNTs is that during loading the individual tubes tend to pull out from the ropes (bundles), thus making load transfer difficult. Therefore, the composite reinforcement is dominated by the collective behavior of the bundles rather than by the strength of individual tubules.[9,14,25,26] As far as the MWNTs are concerned, it is noteworthy that MWNTs produced using the arc-discharge apparatus are highly crystalline and defect-free (absence of vacancies, interstitials, dangling bonds), and the surface is inert so that polymers do not attach firmly to it. Thus, the introduction of defects via oxidation routes using strong acids or the use of pyrolytically carbon-grown nanotubes (containing defects and kinks) may be an alternative to fabricate composites in which the tube surface is strongly bonded to the polymeric matrix.[14] It has been confirmed that refluxing CNTs with concentrated nitric acid creates acidic sites on CNTs, such as carboxylic, carbonyl, and hydroxyl groups.[27−29] These reactive groups on CNTs greatly enhance the combination of CNTs with polymeric matrix, thus improving the mechanical strength of the nanocomposites.[30] Sidewall functionalization of CNTs with organic chains or functional groups is another efficient way to improve the dispersion and strengthen the combination of CNTs with a polymeric matrix.[24,31,32]

There are several main methods reported for preparation of CNTs/polymer composites: (i) solution-casting,[8,33−35] (ii) melt-mixing,[13,36] and (iii) in situ polymerization of monomers with presence of CNTs.[37,38] With the solution-casting method, high-energy sonication of the CNTs suspensions over prolonged periods of time[33,34] or the use of ultrasonic head[35] is usually necessary to produce uniformly dispersed CNTs suspensions before they are subsequently mixed with polymer solutions. Gong et al.[39] and Wei et al.[40] have demonstrated that the presence of nonionic surfactants during processing of epoxy composites (containing 1 wt % of

---

[†] Present address: Institute of Advanced Materials, Fudan University, 220 Handan Road, Shanghai 200433, P. R. China.

[*] To whom correspondence should be addressed. Tianxi Liu: e-mail liu-tx@imre.a-star.edu.sg; Tel +65-68748594; Fax +65-67744657. Wei-De Zhang: e-mail wd-zhang@imre.a-star.edu.sg; Tel +65-68741993; Fax +65-68720785.

10.1021/ma049132t CCC: $27.50

MWNTs) improves the dispersion and strengthens the interactions between the nanotubes and the matrix, thus increasing the elastic modulus by more than 30%. Recently, Xu et al. also showed that 0.1 wt % of MWNTs in epoxy resins increases the elastic modulus by 20%.[41] Dickey and his colleagues reported that addition of 1−5 wt % MWNTs into polystyrene by a simple solution-evaporation method results in 36−42% and 25% increases in elastic modulus and break stress, respectively.[33] Windle et al. prepared the CNTs/poly(vinyl alcohol) composite films with a wide range of CNTs loadings (10−60 wt %) by mixing aqueous poly(vinyl alcohol) solution with CNTs dispersions followed by subsequent casting and controlling evaporation, and the thermomechanical and electrical transport tests were also performed.[8] Bower et al. fabricated CNTs/polyhydroxyaminoether by solution casting and embedded aligned MWNTs in polymer matrices in order to demonstrate the good adherence of the tube surface to the polymer. They studied the deformation of CNTs in the composites and reported that the onset buckling strain and fracture strain were estimated to be 5% and >18%, respectively.[7] Although some MWNTs fracture, most eventually debond at the MWNTs/polymer interface and subsequently are pulled out from the polymer matrix, indicating a weak interfacial interaction between the nanotubes and the matrix.[42] Therefore, the improvement in mechanical properties of the reported polymer nanocomposites with small amounts of CNTs as fillers is usually limited, mainly due to formation of severe CNTs agglomeration and/or poor interfacial interaction with the matrix.

Specified to nylon-6 (PA6), a very important engineering plastic, to avoid the impediment of growing polymer chains due to the presence of CNTs, Jia et al. reported an improved in situ process to enhance the interfacial adhesion between the CNTs and PA6 matrix; however, the improvement in mechanical properties is still very limited, only by about 20%.[43,44] Recently, Xia et al. prepared MWNTs/PA6 composites by microemulsion approach.[45] And most recently, we reported to successfully prepare MWNTs/PA6 nanocomposites by simple melt-compounding method.[46] The aim of the present report is to investigate the morphologies, mechanical properties, and crystallization/melting behavior of MWNTs/PA6 composites in detail.

Experimental Section

Materials and Sample Preparation. Nylon-6 (PA6) pellets (Grade SF1080A) used in this study are the product of Ube Industries under license from Toyota. The MWNTs were prepared by catalytic chemical vapor deposition (CVD) of methane on Co−Mo/MgO catalysts.[47,48] The as-prepared MWNTs were purified by dissolving the catalyst in hydrochloride acid followed by refluxing in 2.6 M nitric acid for increasing more carboxylic and hydroxyl groups, which has been described in detail elsewhere.[49] PA6 composites containing different MWNTs contents (from 0 to 2 wt %) were prepared via a melt-compounding method using a Brabender twin-screw mixer at 250 °C for 10 min with a screw speed of 100 rpm. Film samples (with thickness of about 0.5 mm) were prepared by compression molding in a press at a temperature of 250 °C with a pressure of 150 bar, followed by quickly quenching in an ice/water bath.

Microscopy Characterization. A field emission scanning electron microscope (SEM) (JEOL JSM 6700F) was used to observe the purified MWNTs and the morphology of the failure surfaces (after tensile tests) of the CNTs/PA6 composites. Transmission electron microscopy (TEM) observation of MWNTs was performed with a Philips CM300 FEG TEM instrument operated under an acceleration voltage of 300 kV. Thin sections (with thickness of about 70 nm) for TEM observations were cut from the as-prepared composites under cryogenic conditions using a Leica ultramicrotome with a diamond knife.

X-ray Diffraction. The X-ray diffraction (XRD) patterns were recorded using a Brüker GADDS diffractometer with 2D area detector operating under a voltage of 40 kV and a current of 40 mA using Cu Kα radiation ($\lambda = 0.154\ 18$ nm).

Thermal Analysis. Differential scanning calorimetry (DSC) experiments were performed in a DSC-2920 from TA Instruments coupled with a TA-2000 control system. The samples were heated at a scanning rate of 10 °C/min under a nitrogen atmosphere in order to diminish oxidation. Dynamic mechanical analysis (DMA) was performed on the samples of $30 \times 10 \times 0.5$ mm^3 in size using a dynamic mechanical analyzer from TA Instruments under tension film mode in a temperature range of ambient to 200 °C at a frequency of 1 Hz and heating rate of 3°/min.

Tensile Testing. The quenched films were finally punched into dog-bone specimens with a dimension of $63.5 \times 9.53 \times 3.18$ mm^3 (Die ASTM D-638 type V) using a CEAST hollow die punch (model 6051). The tensile tests were carried out using an Instron universal material testing system (model 5567) at room temperature with gauge length of 25 mm and crosshead speed of 5 mm/min. Property values reported here represent an average of the results for tests run on at least six specimens.

Nanoindentation Tests. The nanoindentation tests were performed on MTS Nano Indenter XP (MTS Corp., Nano Instruments Innovation Center, TN) with a continuous stiffness measurement technique.[50] In this technique, a small sinusoidal load with known frequency and amplitude was superimposed onto the quasi-static load. It results in a modulation of the indenter displacement that is phase shifted with respect to the excitation force. The materials stiffness (S) and damping (ωC) along indentation loading can be calculated using eqs 1 and 2, respectively. The hardness and elastic modulus are calculated using stiffness data from eqs 3 and 4, respectively. Therefore, the hardness and modulus are determined as a function of indentation depth with a single loading/unloading cycle.[51]

$$S = \left[\frac{1}{\dfrac{P_{\max}}{h(\omega)}\cos\Phi - (K_s - m\omega^2)} - K_f^{-1}\right]^{-1} \tag{1}$$

$$\omega C = \frac{P_0}{h(\omega)}\sin\Phi \tag{2}$$

$$\frac{E}{1-\nu^2} = \frac{\sqrt{\pi}}{2}\frac{1}{\sqrt{A_c}}S \tag{3}$$

$$H = \frac{P_{\max}}{A_c} \tag{4}$$

where $P_{\max}$ and $h(\omega)$ are driving force and the displacement response of the indenter, respectively; Φ is the phase angle between $P_{\max}$ and $h(\omega)$; m is mass of the indenter column; K_s is spring constant at the vertical direction; K_f is frame stiffness; m, K_s, and K_f are all constant values for specified indentation system; ω is angle speed which equals to $2\pi f$; f is the driven frequency of the ac signal, which is 45 Hz for present study; ν is Possion's ratio and set to be 0.35 for current analysis; and A_c is contact area at the moment material in contact with indenter with load $P_{\max}$.

A three-side pyramid (Berkovich) diamond indenter was employed for the indentation experiments. The area function, which is used to calculate contact area A_c from contact depth h_c, was carefully calibrated using standard sample, fused silica, before the experiments. The nanoindentation tests were carried out in the following sequence: First, the indenter was

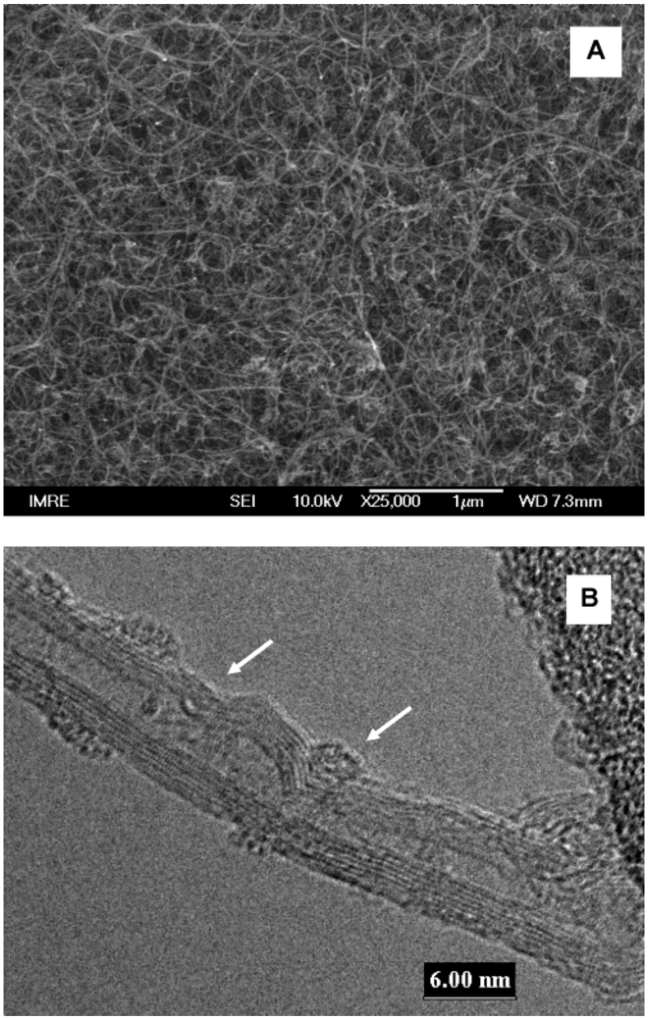

Figure 1. (A) Typical SEM image showing the morphology of MWNTs. (B) Typical TEM image illustrating the graphitic layer structure of a MWNT with curvature and defects on one side of the CNTs at higher magnification.

brought into contact with the surface at a constant strain rate, i.e., 0.05 1/s, until 5000 nm of penetration was achieved. The load was then held at the maximum value for 60 s in order to determine the creep behavior. The indenter was then withdrawn from the surface at the same rate until 10% of the maximum load was reached. A constant strain rate was chosen to load the samples in order to avoid the strain-hardening effect on the measurements. A minimum of 10 indents was performed on each sample, and the distance between indentations was 50 μm to avoid interactions.

Results and Discussion

Morphology and Dispersion of CNTs. The SEM image of the purified and acid-treated MWNTs is shown in Figure 1A. It can be seen that the tubes are randomly and loosely entangled together without any particle-like impurities. The MWNTs were observed to be several nanometers to 20 nm in thickness and several tens microns in length by dispersing the extremely diluted solution. Figure 1B shows the TEM image of a typical MWNT with thickness of about 7 nm, and its sidewall contains eight graphitic layers. One can clearly see the curvature and defect (indicated by arrows) on one side of the wall. These kinds of observable defects, together with many other defects, such as vacancies, dangling bonds, interstitials, pentagon and heptagon pairs in the carbon framework, etc., usually exist on the MWNTs prepared by the CVD method. The defects on the MWNTs are the most active locations for chemical or physical functionalization of the CNTs.[52]

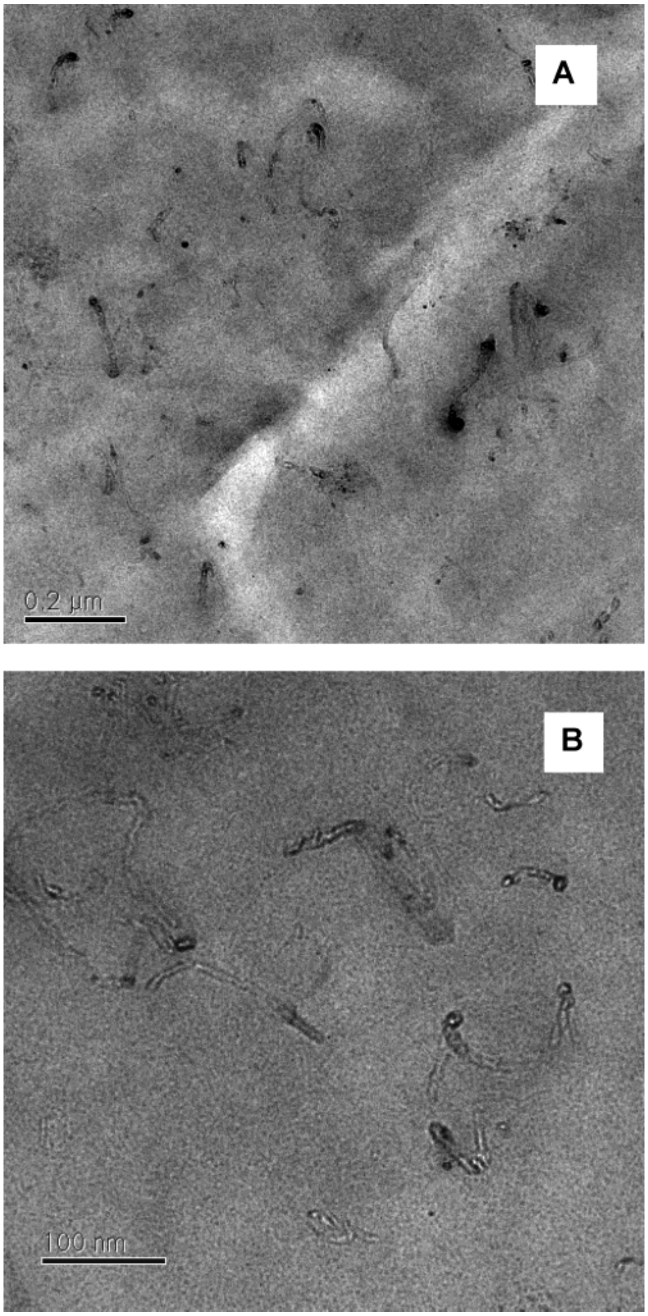

Figure 2. TEM images showing nanotube dispersion from the ultrathin section of PA6 nanocomposite containing 1 wt % MWNTs: (A) low magnification; (B) high magnification.

TEM observation (Figure 2) shows fine and homogeneous dispersion of MWNTs throughout PA6 matrix, as an example, for the ultrathin section of the nanocomposite containing 1 wt % CNTs. The variations in contrast and diameter of the CNTs are mainly due to difference in electron scattering from different depth regions of the section. From Figure 2A, individual CNTs are randomly dispersed (without preferred alignment or orientation after melt-compounding) within the matrix, and no CNTs aggregation is observed. At higher magnification (Figure 2B), the intriguing feature is that most CNTs remain curved or even interwoven in the composite, indicating extreme flexibility of nanotubes. The embedded CNTs seldom appear as straight inclu-

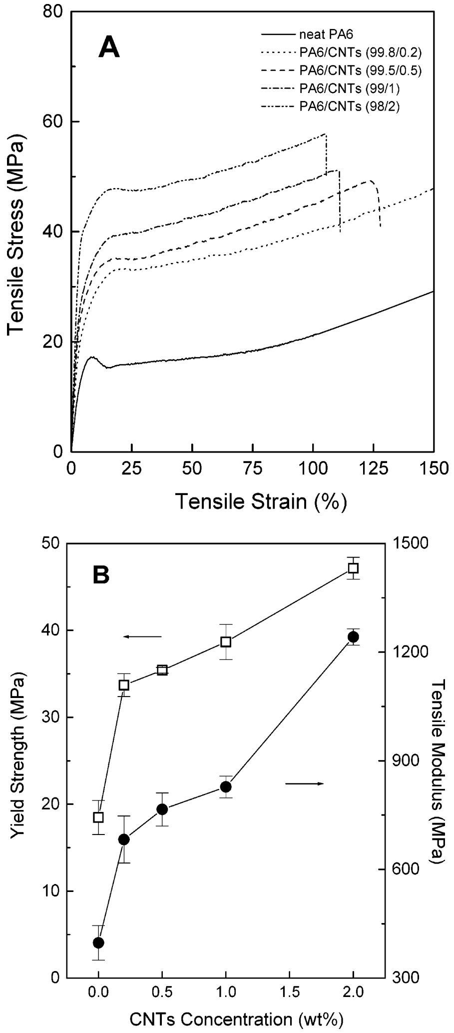

Figure 3. (A) Typical stress–strain curves. (B) Tensile stress (at yield) and tensile modulus for PA6 and its nanocomposites as a function of MWNTs concentration.

sions but are rather often characterized by a certain degree of waviness or entanglements along their axial dimension. Such curvature or knotting significantly reduces the structural reinforcement that the CNTs provide the host polymer matrix, in comparison to the theoretical reinforcement provided by straight inclusion, as pointed out by Fisher et al.[53] And, since some nanotubes seem to point out of the section surface, one can even observe the ends (i.e., cross sections) of individual CNTs embedded in the matrix due to cutting by the ultramicrotome. In addition, because of the pronounced curved morphology of CNTs, some parts of the tubes are cut during TEM sample preparation and thus appear as several individual tubes. Clearly, microtoming does not affect the intimate adhesion of CNTs with the matrix, indicating good wettability between them, as observed in the epoxy/nanotube composites.[15]

Tensile Property and Reinforcement Mechanisms. Typical stress–strain curves for neat PA6 and MWNTs/PA6 composites with different CNTs loadings are shown in Figure 3A. A pronounced yield and postyield drop are observed for neat PA6, while there is almost no noticeable yield for MWNTs-reinforced PA6 composites. It can be seen that the tensile properties of the composites significantly increase with increasing the loading level of the nanotubes, as presented in Figure 3B. Upon incorporation of only 2 wt % MWNTs, the elastic modulus of PA6 is greatly improved by about 214% from 396 to 1242 MPa, and the yield strength is improved by about 162% from 18 to 47 MPa. The elongation at break (about 110%) slightly decreases, indicating that the composite becomes somewhat brittle compared with neat PA6 (which breaks at above 150% of elongation).In addition, Figure 3 shows a remarkable enhancement in the toughness of neat PA6 by incorporating CNTs. The possible toughening mechanism(s) will be discussed later by SEM observations. Moreover, it is worth comparing the mechanical properties of PA6/MWNTs composites prepared here with those of PA6/clay nanocomposites reported in the literature. Upon incorporating 4.7 wt % montmorillonite into PA6 matrix, the tensile modulus and strength are only improved by about 68% and 42%, respectively.[54] Thus, the advantages and uniqueness of using the CNTs as reinforcing nanofillers to make polymer nanocomposites are obvious.

To reveal the possible reinforcing mechanism(s), the failure surfaces of PA6/MWNTs composites after tensile testing were investigated in detail by SEM. Figure 4A shows a typical overview on the fracture surfaces of the composite containing 0.5 wt % MWNTs. The uniformly dispersed bright dots and lines are the ends of the broken MWNTs. SEM image clearly shows that an even dispersion of MWNTs is achieved throughout the PA6 matrix. Clearly, most MWNTs are separated into individual tubes by shear force from simple melt-blending and thus evenly dispersed in the matrix, which is of great importance for making CNTs reinforced polymer composites with excellent mechanical properties. Moreover, close inspection indicates that upon failure most of the MWNTs were broken apart, while a few were pulled out of the matrix, as shown in Figure 4B. A nanotube, as indicated by arrow 1 in Figure 4B, was observed to be broken, with the other two ends still strongly embedded in the matrix. This interesting and typical breakage phenomenon of the CNTs upon tensile stretching indicates a strong interfacial adhesion between MWNTs and PA6 matrix and a sufficient load transfer from the polymer to nanotubes. It is thus believed that the strong interfacial adhesion observed above is responsible for the significant improvement of mechanical property shown in Figure 3. In addition, another beltlike nanotube was observed which interconnects two polymer lumps, as indicated by arrow 2. Obviously, this interconnection is realized by an individual tube or bundle of MWNTs wrapped by the matrix since its diameter is much bigger than other broken tubes (i.e., bright dots) observed on the fracture surface. Moreover, the middle part of the tube is smaller than the two ends adhered to the two lumps of polymeric matrix. This also indicates that the interconnection of MWNTs with PA6 matrix is very strong.

Furthermore, to illustrate fracture behavior and possible toughening mechanisms, close and detailed investigations were performed on some representative fractured regions of the nanocomposites after tensile tests. Figure 4C shows a typical fracture surface of the nanocomposite. It can be seen that the nanotubes are not simply or entirely pulled out but fully stretched during the deformation and failure processes of the composites. Most stretched nanotubes or bundles are well aligned, clearly indicating that stretching can align CNTs or their bundles easily, as observed by other researchers.[4,9,15] And, the well-aligned nanotubes and

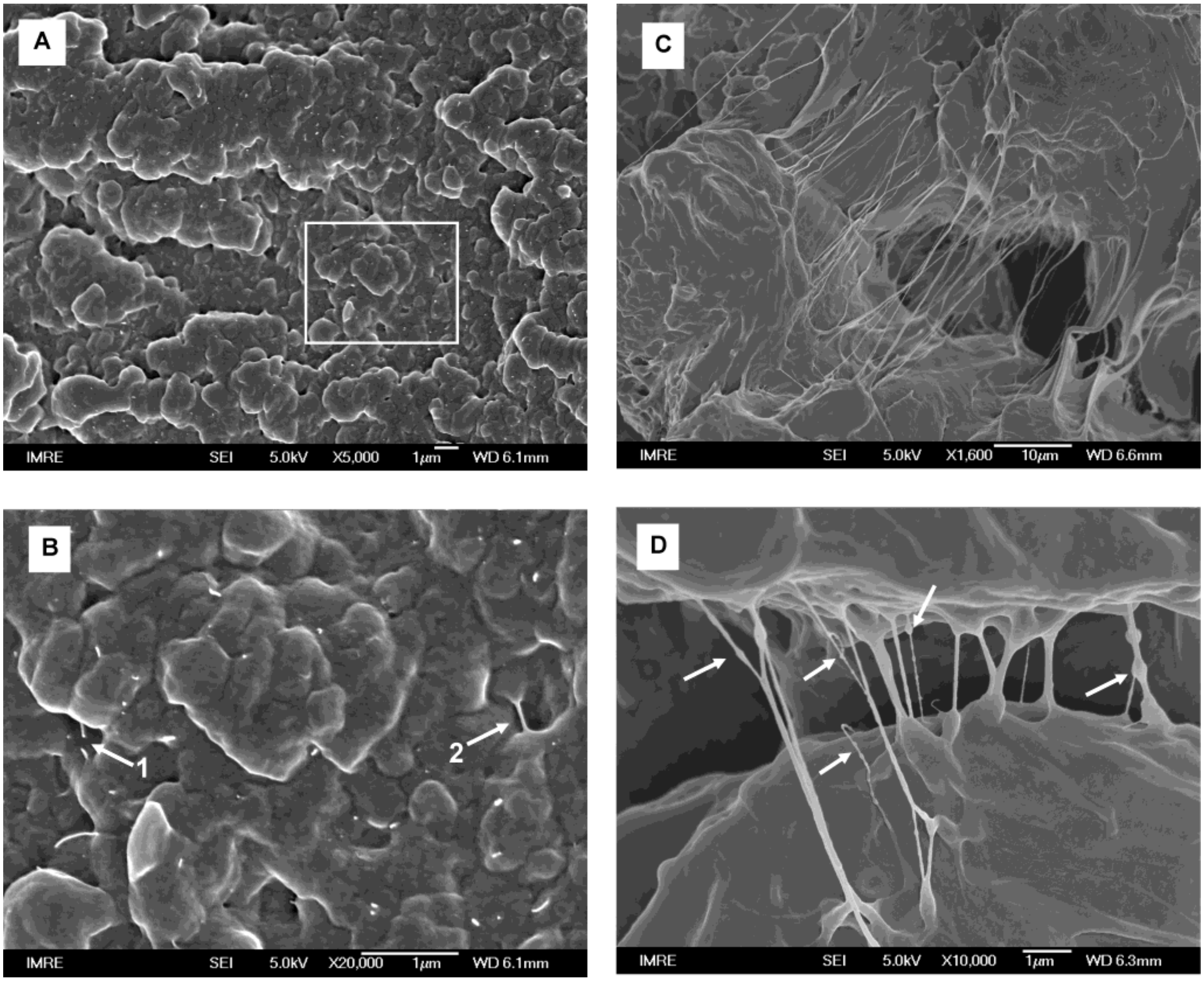

Figure 4. (A) SEM image showing an overall morphology of failure surface for PA6 nanocomposite containing 0.5 wt % MWNTs. (B) Enlarged morphology of selected region in (A). (C) SEM image showing microcracks linked by stretched nanotubes and their bundles in PA6 nanocomposites. (D) Enlarged SEM image of the microcrack connected by MWNTs sheathed with polymer in PA6 nanocomposites. Some MWNTs are sheathed by several small polymer beads.

Table 1. Summary of Mechanical Properties of Neat PA6 and Its Nanocomposites as a Function of CNTs Concentration

	neat PA6	PA6/CNTs (99.8/0.2)	PA6/CNTs (99.5/0.5)	PA6/CNTs (99/1)	PA6/CNTs (98/2)
yield strength (MPa)	18.0 ± 2.2	33.7 ± 1.3	35.4 ± 0.3	40.3 ± 3.1	47.2 ± 1.2
tensile modulus (GPa)	396.0 ± 36.6	682.5 ± 65.0	765.5 ± 45.9	852.4 ± 77.0	1241.8 ± 22.8
modulus (GPa)[a]	2.08	2.55	2.57	3.14	2.97
modulus (GPa)[b]	1.18 ± 0.02	1.33 ± 0.03	1.60 ± 0.12	2.02 ± 0.02	
hardness (GPa)	0.06 ± 0.001	0.08 ± 0.005	0.10 ± 0.005	0.11 ± 0.003	

[a] Modulus at 0 °C obtained by DMA. [b] Modulus obtained from nanoindentation tests.

their bundles bridge across the cracks (Figure 4C), which allows the release of stress and absorbs the fracture energy, thus contributing to toughness improvement. However, it is also observed that some of them become loosened or curved, probably due to (i) relaxation after fracture or (ii) uneven crack separation. The latter is due to the fact that typically during fracture the crack opens, stretches the reinforcing nanotubes, and subsequently closes (relax) somewhat, removing the load on the nanotubes.[9]

Very interestingly, a bead- or ball-like morphology along the stretched nanotubes or the bundles (as bridges across the microcrack) is observed under close inspection at higher magnification, as indicated by white arrows (Figure 4D). It is reasonably believed that these beads are the absorbed matrix protruding or layers around MWNTs, showing the intimate contact and good adherence of the polymer to the nanotubes.[7,13] The locations of the beads must be closely related to the sites of the (active) defects or imperfections along the nanotubes or their bundles. Similar ball-like morphology along CNTs (covered with a layer of polymer) was also observed by Zhou and co-workers.[7]

Thermomechanical Property by DMA. Figure 5 shows the DMA curves as a function of CNTs concentration, and the elastic modulus data are summarized in Table 1. It can be seen that with increasing CNTs loading level the storage moduli of the nanocomposites increase gradually. The storage modulus (2.97 GPa) for the nanocomposite containing 2 wt % CNTs exhibits

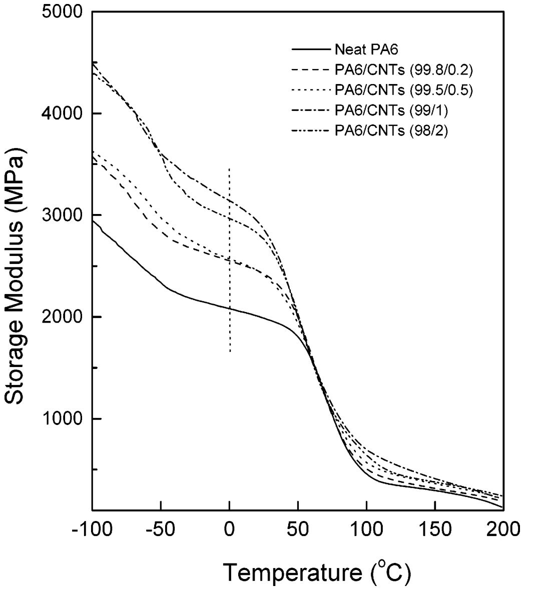

Figure 5. Storage modulus vs temperature (DMA) curves for PA6 and its nanocomposites as a function of MWNTs concentration.

43% increment compared with neat PA6 (2.08 GPa) within the glassy plateau (at 0 °C) and increases by about 57% within the rubbery plateau (at 120 °C) from 350 MPa (for neat PA6) to 550 MPa (for the nanocomposite with 2 wt % CNTs). The significant improvement in storage modulus of PA6/CNTs nanocomposites is ascribed to the combined effect of high performance and fine dispersion of high aspect ratio CNTs filler. The glass transition temperature (T_g) remains almost unchanged at about 65 °C upon incorporating MWNTs into PA6 matrix, probably indicating that less constraints from one-dimensional (1D) CNTs nanofiller are imposed on the polymer chains. This is different from the case usually reported in 2D layered silicates (e.g., clay) reinforced polymer nanocomposites,[54] where the mobility of polymer chains is greatly constricted by confinement effect from 2D nanoclay platelets, thus usually increasing the T_g of the nanocomposites.[55,56]

Nanoindentation Behavior. Figure 6A shows typical loading–hold–unloading curves of neat PA6 and its nanocomposites as a function of CNTs content. It is immediately clear that the mechanical responses of neat PA6 and the composites differ considerably. On loading, the forces are incremented at constant velocities. The curves steadily shift upward with increasing the CNTs concentration, indicating that the nanocomposite's resistance to indentation gradually increases with nanotube concentration. The depths represent the contributions from both the elastic and the plastic displacements. The loading curves are followed by a period of holding time (here, 60 s) at which the peak loads are kept constant. During unloading, the load is reduced at the same rate as in the loading cycle. In this case, the elastic displacements are recovered. It can be seen that significant creep was clearly found in the maximum hold segments for both neat PA6 and the nanocomposites. However, the (creep) depths or displacements at maximum holding segments show no distinct difference with increasing CNTs content, suggesting that incorporation of nanotube has little effect on the viscoelastic property of the PA6 matrix and does not affect the creep resistance of the material.

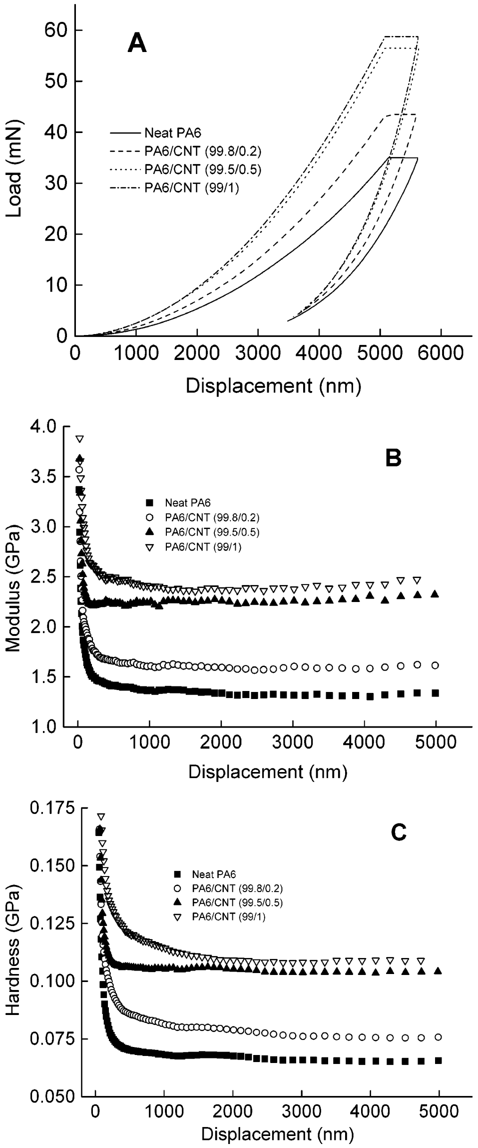

Figure 6. (A) Typical loading-unloading curves. (B, C) Modulus and hardness profiles with respect to displacement into sample surfaces for neat PA6 and its nanocomposites as a function of MWNTs content.

Parts B and C of Figure 6 show the modulus (E) and hardness (H) profiles with respect to the indentation depth, respectively, for neat PA6 and its composites as a function of MWNTs concentration. It can be seen that both the elastic modulus and the hardness are significantly improved by about 84% upon loading only 1 wt % CNTs, compared with neat PA6 matrix, as summarized in Table 1. The results of H and E in Table 1 are averaged values in the depth between 4000 and 5000 nm. The dramatic drops of the hardness and the modulus before 200 nm are probably due to the indentation size effect (ISE).[57] Several possible origins for the ISE are discussed elsewhere.[58] After indentation depth approaches 200 nm and onward, the profiles show stable trends for all the samples, indicating that MWNTs are homogeneously dispersed along the indentation direction.

Additionally, it can be seen from Table 1 that the modulus data by three techniques (i.e., tensile testing, DMA, and nanoindentation) have the same changing tendency but with different absolute values. The possible origins for the discrepancy may be due to the different loading directions and the frequency used for the three measurements. For a tensile test, the loading direction on the samples is perpendicular to the compression molding direction, while the loading direction for the indentation measurement is along with the compression molding direction. When most polymer chains align or orient along the molding direction, the modulus measured in that direction is expected to be higher than other directions. It is also known that for polymers the frequency used during testing will affect the viscoelastic properties of the materials. Usually, the higher frequency used, the lower modulus obtained. In DMA measurement, low frequency (e.g., 1 Hz in this study) was usually used. However, for the present indentation test, the frequency of 45 Hz was used. Thus, it is expected that the measured mechanical properties of PA6 and its composite systems have some differences from the three methods used here.

In summary, the mechanical properties of the prepared MWNTs/PA6 composites increase significantly with addition of only small amount (≤2 wt %) of MWNTs into the PA6 matrix. The high performance of the composites is attributed to homogeneous dispersion of MWNTs in the matrix as well as the strong interfacial interaction between MWNTs and polymeric matrix. As indicated in the Experimental Section, the MWNTs have been refluxed in diluted (2.6 N) nitric acid for creating carboxylic and hydroxyl groups.[49] It is worthy to point out that the treated MWNTs are still in a loose form (Figure 1A). They are quite different from those oxidized in concentrated acids, which are highly packed and cannot be dispersed again in the solvent after drying (probably due to the presence of too much carboxylic and hydroxyl groups and thus strong interactions with the CNTs).[59] Loose accumulation will be advantageous for the dispersion of MWNTs in the polymeric matrix, while functionalization of the MWNTs with $-$COOH groups will increase the anchoring (or interacting) sites along the nanotubes with polymeric matrix, thus being favorable to stress transfer from polymer to CNTs. The hydrophilic functional groups on the MWNTs are helpful for improving the interaction with PA6, which possesses polar $-$CONH$-$ groups along the polymer chains.[32] Therefore, the compatibility and strong interaction between the MWNTs fillers and the matrix greatly enhance the dispersion as well as the interfacial adhesion, thus strengthening the overall mechanical performance of the composites.

Melting and Crystallization Behavior by DSC and XRD. To investigate the effect of CNTs addition on the crystallization and melting behavior of PA6, DSC and XRD studies are performed comparatively. Figure 7A illustrates the effect of crystallization or annealing temperature (T_c) on the thermal behavior of neat PA6 melt-crystallized at indicated temperatures ($T_g = 65$ °C $< T_c < T_m$ (melting point) $= 225$ °C for PA6). It can be observed that, in the main melting region (i.e., in the temperature range 200−230 °C) of PA6, there are two melting peaks, $T_{m,1}$ (at about 214 °C) and $T_{m,2}$ (at about 223 °C), corresponding to the melting events of γ-form and α-form crystals, respectively.[60−63] The positions of the $T_{m,1}$ and $T_{m,2}$ are relatively constant with increasing T_c. It has been well-documented that for PA6 the α crystalline phase is thermodynamically stable and consists of sheets of hydrogen-bonded chains formed between antiparallel chains; the γ crystalline phase is metastable and consists of random hydrogen bonding between parallel chains.[64,65] It indicates that the formation of γ-crystals is preferred at low temperature (e.g., at 80 and 120 °C), whereas the α-form population is dominant at higher temperatures. At lower T_c (e.g., below 160 °C), an exothermic peak at about 200 °C can be observed, probably indicating that some uncrystallizable materials may undergo a reorganization or recrystallization during the heating process in DSC. Such a recrystallization process during heating is significantly prohibited at higher T_c (e.g., for $T_c = 200$ °C) due to improved perfection in the crystals formed. At an even higher annealing temperature (e.g., $T_c \geq 200$ °C), the double melting peaks ($T_{m,1}$ and $T_{m,2}$) merge into one at about 220 °C. Another endothermic peak (indicated by arrows), the so-called "annealing peak" (T_a), can be induced by isothermal crystallization or annealing process for neat PA6. The position of the T_a shifts toward higher temperatures (always about 10 °C above the T_c) accompanied by an increasing magnitude as the T_c increases. It should be noted that this annealing-induced endotherm is a universal phenomenon in most semicrystalline thermoplastic polymers, such as poly(aryl ether ether ketone), poly(phenylene sulfide), poly(ethylene terephthalate),[66] isotactic polystyrene.[67−70]

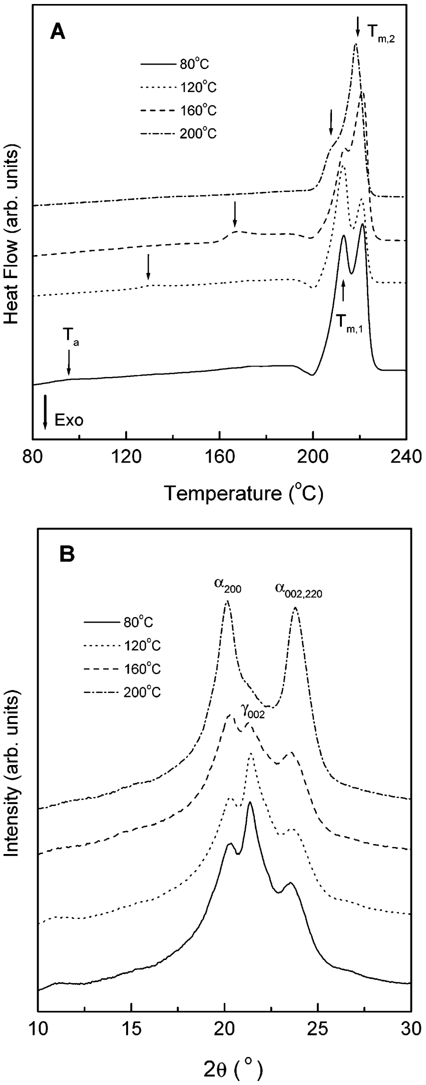

Figure 7. (A) DSC heating curves for neat PA6 samples annealed at indicated temperatures for 2 h. (B) XRD patterns for neat PA6 samples having the same thermal history as in (A) prior to DSC runs.

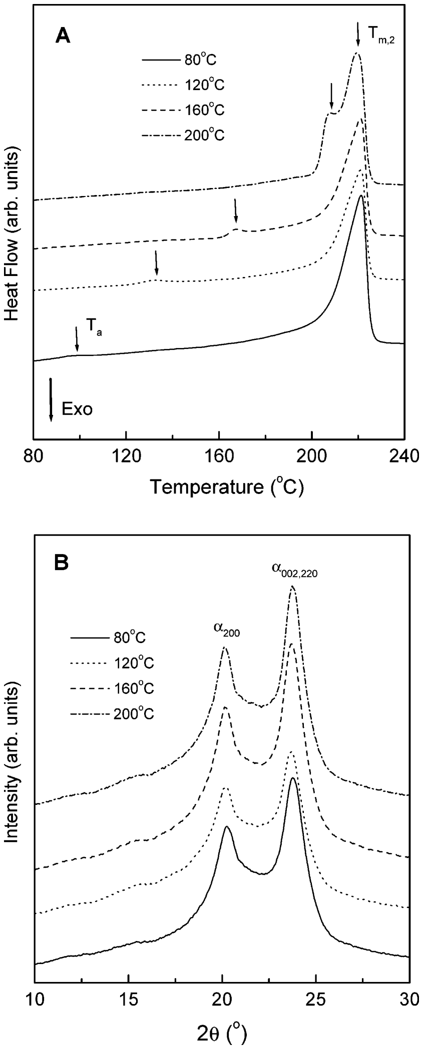

Figure 8. (A) DSC heating curves and (B) XRD patterns for PA6 nanocomposite containing 1 wt % MWNTs having the same thermal history as in Figure 7.

The possible physical origins of this behavior are still under debate in the literature and beyond the research scope of the present study.

The corresponding XRD patterns (Figure 7B) are well consistent with the DSC results presented in Figure 7A. At lower T_c, the coexistence of α-form (i.e., (200) and (002, 220) reflections at $2\theta = 20°$ and 23.7°, respectively) and γ-form crystals (i.e., (001, 200) reflection at $2\theta = 21.4°$) are clearly observed, as reported previously in the literature for neat PA6.[61,62,65] The α-phase crystals gradually become a dominant population with increasing the T_c, at the expense of the γ-phase crystals. However, the melting and crystallization behaviors of the CNTs reinforced PA6 nanocomposites; as an example, the one containing 1 wt % MWNTs (Figure 8) is different from those of neat PA6 (Figure 7). From DSC results shown in Figure 8A, in addition to the so-called annealing peak (T_a) as indicated by arrows, only the high-temperature melting peak ($T_{m,2}$) is observed at about 220 °C for all the annealed composite samples, probably indicating that only the α-form crystals (related to the $T_{m,2}$) are formed upon addition of nanotubes into PA6 matrix. This speculation has been further confirmed by XRD results, as illustrated in Figure 8B.

Very interestingly, the above features observed by DSC and XRD are totally different from those always observed in PA6/clay nanocomposites, where the addition of nanoclay filler inevitably induces the formation of the γ-phase crystals, as evidenced by a number of detailed studies.[62,63,65,71,72] It is proposed that the presence of 2D layered clay sheets disrupts the α-crystallite formation and results in the less-ordered γ-phase crystals.[67] Thus, the confined environment and specific interfacial interactions provided by the 2D disklike nanoclay platelets are probably responsible for the formation of less stable γ-phase crystals. However, for the case of MWNTs-filled PA6 composites, the nanoscale confinement effect from the 1D geometry nanotubes on the crystallization of PA6 matrix seems much less compared with that of nanoclay platelets. That is, the constraints from the CNTs imposed on the polymer chains are much less than those from the nanoclay sheets. The nanotubes may only provide the nucleation sites for end-tethering of PA6 chains to form the α-phase crystals. And, it is reported that the α-phase crystals of PA6 exihibits a higher modulus than the γ-phase,[65] which may also be one of the roots of the property enhancements observed here in MWNTs/PA6 composites. Clearly, detailed studies need to be conducted to fully understand the effect of CNTs addition on the crystalline morphology and crystallization mechanism(s) of PA6.

Conclusions

MWNTs-reinforced PA6 nanocomposites with excellent mechanical properties have been successfully prepared by simple melt-compounding method. Systematic studies using different mechanical tests (such as tensile and nanoindentation methods) show that incorporation of a small amount of MWNTs into PA6 matrix can significantly improve the modulus, the strength, and the hardness by about 214%, 162%, and 83%, respectively, with less than 2 wt % CNTs. Microscopy observations indicate that a uniform and fine dispersion of MWNTs throughout PA6 matrix and a strong interfacial adhesion between nanotubes and the matrix have been successfully achieved, which are responsible for the remarkable enhancements in overall mechanical properties of the nanocomposites prepared. DSC and XRD results show that the effect of MWNTs addition on the crystallization and melting behavior of PA6 matrix is greatly different from the case of addition of clay, probably due to the difference in geometry or morphology of nanofillers used. Detailed studies on the crystallization mechanism(s) of PA6 upon incorporation of CNTs are currently under investigation.

References and Notes

(1) Baughman, R. H.; Zakhidov, A. A.; de Heer, W. A. *Science* **2002**, *297*, 787−792.
(2) Collins, P. G.; Avouris, P. *Sci. Am.* **2000**, *Dec*, 62−69.
(3) Wagner, H. D.; Lourie, O.; Feldman, Y.; Tenne, R. *Appl. Phys. Lett.* **1998**, *72*, 188−190.
(4) Jin, L.; Bower, C.; Zhou, O. *Appl. Phys. Lett.* **1998**, *73*, 1197−1199.
(5) Schadler, L. S.; Giannaris, S. C.; Ajayan, P. M. *Appl. Phys. Lett.* **1998**, *73*, 3842−3844.
(6) Laurie, O.; Cox, D. E.; Wagner, H. D. *Appl. Phys. Lett.* **1998**, *81*, 1638−1642.
(7) Bower, C.; Rosen, R.; Jin, L.; Han, J.; Zhou, O. *Appl. Phys. Lett.* **1999**, *74*, 3317−3319.
(8) Shaffer, M. S. P.; Windle, A. H. *Adv. Mater.* **1999**, *11*, 937−941.
(9) Ajayan, P. M.; Schadler, L. S.; Giannaris, C.; Rubio, A. *Adv. Mater.* **2000**, *12*, 750−753.

(10) Haggenmueller, R.; Gommans, H. H.; Rinzler, A. G.; Fischer, J. E.; Winey, K. I. *Chem. Phys. Lett.* **2000**, *330*, 219−225.
(11) Wagner, H. D. *Chem. Phys. Lett.* **2002**, *361*, 57−61.
(12) Cooper, C. A.; Ravich, D.; Lips, D.; Mayer, J.; Wagner, H. D. *Compos. Sci. Technol.* **2002**, *62*, 1105−1112.
(13) Potschke, P.; Fornes, T. D.; Paul, D. R. *Polymer* **2002**, *43*, 3247−3255.
(14) Terrones, M. *Annu. Rev. Mater. Res.* **2003**, *33*, 419−501.
(15) Ajayan, P. M.; Stephan, O.; Colliex, C.; Trauth, D. *Science* **1994**, *265*, 1212−1214.
(16) Dalton, A. B.; Collins, S.; Muñoz, E.; Razal, J. M.; Ebron, V. H.; Ferraris, J. P.; Coleman, J. N.; Kim, B. G.; Baughman, R. H. *Nature (London)* **2003**, *423*, 703−703.
(17) Ago, H.; Petritsch, K.; Shaffer, M. S. P.; Windle, A. H.; Friend, R. H. *Adv. Mater.* **1999**, *11*, 1281−1285.
(18) Roberts, J. A.; Imholt, T.; Ye, Z.; Dyke, C. A.; Price Jr., D. W.; Tour, J. M. *J. Appl. Phys.* **2004**, *95*, 4352−4356.
(19) Goh, H. W.; Goh, S. H.; Xu, G. Q.; Lee, K. Y.; Yang, G. Y.; Lee, Y. W.; Zhang, W. D. *J. Phys. Chem. B* **2003**, *107*, 6056−6062.
(20) Watts, P. C. P.; Hsu, W. K.; Kroto, H. W.; Walton, D. R. M. *Nano Lett.* **2003**, *3*, 549−553.
(21) Barrau, S.; Demont, P.; Peigney, A.; Laurent, C.; Lacabanne, C. *Macromolecules* **2003**, *36*, 5187−5194.
(22) Liao, K.; Li, S. *Appl. Phys. Lett.* **2001**, *79*, 4225−4227.
(23) Zhu, J.; Kim, J. D.; Peng, H.; Margrave, J. L.; Khabashesku, V. N.; Barrera, E. V. *Nano Lett.* **2003**, *3*, 1107−1113.
(24) Mitchell, C. A.; Bahr, J. L.; Arepalli, S.; Tour, J. M.; Krishnamoorti, R. *Macromolecules* **2002**, *35*, 8825−8830.
(25) Barrera, E. V. *J. Miner. Metall. Mater. Soc.* **2000**, *52A*, 38−42.
(26) McCarthy, B.; Coleman, J. N.; Czerw, R.; Dalton, A. B.; Panhuis, M. I. H.; Maiti, A.; Drury, A.; Bernier, P.; Nagy, J. B.; Lahr, B.; Byrne, H. J.; Carroll, D. L.; Blau, W. J. *J. Phys. Chem. B* **2002**, *106*, 2210−2216.
(27) Satishkumar, B. C.; Govindaraj, A.; Mofokeng, J.; Subbanna, G. N.; Rao, C. N. R. *J. Phys. D: Appl. Phys.* **1996**, *29*, 4925−4934.
(28) Kuznetsova, A.; Mawhinney, D. B.; Naumenko, V.; Yates Jr., J. T.; Liu, J.; Smalley, R. E. *Chem. Phys. Lett.* **2000**, *321*, 292−296.
(29) Ebbsen, T. W.; Hiura, H.; Bischer, M. E. *Adv. Mater.* **1996**, *8*, 155−160.
(30) Jang, J.; Bae, J.; Yoon, S. H. *J. Mater. Chem.* **2003**, *13*, 676−681.
(31) Lin, Y.; Hill, D. E.; Bentley, J.; Allard, L. F.; Sun, Y. P. *J. Phys. Chem. B* **2003**, *107*, 10453−10457.
(32) Koshio, A.; Yudasaka, M.; Zhang, M.; Iijima, S. *Nano Lett.* **2001**, *1*, 361−363.
(33) Qian, D.; Dickey, E. C.; Andrews, R.; Rantell, T. *Appl. Phys. Lett.* **2000**, *76*, 2868−2870.
(34) Safadi, B.; Andrews, R.; Grulke, E. A. *J. Appl. Polym. Sci.* **2002**, *84*, 2660−2669.
(35) Pirlot, C.; Willems, I.; Fonseca, A.; Nagy, J. B.; Delhalle, J. *Adv. Eng. Mater.* **2002**, *4*, 109−114.
(36) Andrews, R.; Jacques, D.; Minot, M.; Randell, T. *Macromol. Mater. Eng.* **2002**, *287*, 395−403.
(37) Wu, W.; Zhang, S.; Li, Y.; Li, J.; Liu, L.; Qin, Y.; Guo, Z. X.; Dai, L.; Ye, C.; Zhu, D. *Macromolecules* **2003**, *36*, 6286−6288.
(38) Qin, S.; Qin, D.; Ford, W. T.; Resasco, D. E.; Herrera, J. E. *J. Am. Chem. Soc.* **2004**, *126*, 170−176.
(39) Gong, X.; Liu, J.; Baskaran, S.; Voise, R. D.; Young, J. S. *Chem. Mater.* **2000**, *12*, 1049−1052.
(40) Wei, C. Y.; Strivastava, D.; Cho, K. J. *Nano Lett.* **2002**, *2*, 647−650.
(41) Xu, X. J.; Thwe, M. M.; Shearwood, C.; Liao, K. *Appl. Phys. Lett.* **2002**, *81*, 2833−2835.
(42) Qian, D.; Dickey, E. C. *J. Microsc.* **2001**, *204*, 39−45.
(43) Jia, Z.; Xu, C.; Liang, J.; Wei, B.; Wu, D.; Zhu, C. *Xinxing Tan Cailiao* **1999**, *14*, 32−36.
(44) Jia, Z.; Wang, Z.; Xu, C.; Liang, J.; Wei, B.; Wu, D.; Zhang, Z. *Qinghua Daxue Xuebao, Ziran Kexueban* **2000**, *40*, 14−16.
(45) Xia, H.; Wang, Q.; Qiu, G. *Chem. Mater.* **2003**, *15*, 3879−3886.
(46) Zhang, W. D.; Shen, L.; Phang, I. Y.; Liu, T. X. *Macromolecules* **2004**, *37*, 256−259.
(47) Bacsa, R. R.; Laurent, C.; Peigney, A.; Bacsa, W. S.; Vaugien, T.; Rousset, A. *Chem. Phys. Lett.* **2000**, *323*, 566−571.
(48) Flahaut, E.; Peigney, A.; Laurent, C.; Rousset, A. *J. Mater. Chem.* **2000**, *10*, 249−252.
(49) Goh, H. W.; Goh, S. H.; Xu, G. Q.; Pramoda, K. P.; Zhang, W. D.*Chem. Phys. Lett.* **2003**, *379*, 236−241.
(50) Lucas, B. N.; Oliver, W. C.; Swindeman, J. E. *Mater. Res. Soc. Symp. Proc.* **1998**, *522*, 3−14.
(51) Oliver, W. C.; Pharr, G. M. *J. Mater. Res.* **1992**, *7*, 1564−1583.
(52) Hirsch, A. *Angew. Chem., Int. Ed.* **2002**, *41*, 1853−1859.
(53) Fisher, F. T.; Bradshaw, R. D.; Brinson, L. C. *Appl. Phys. Lett.* **2002**, *80*, 4647−4649.
(54) Kojima, Y.; Usuki, A.; Kawasumi, M.; Okada, A.; Fukushima, Y.; Kurauchi, T.; Kamigaito, O. *J. Mater. Res.* **1993**, *8*, 1185−1189.
(55) Krishnamoorti, R.; Vaia, R. A.; Giannelis, E. P. *Chem. Mater.* **1996**, *8*, 1728−1734.
(56) Lu, H. B.; Nutt, S. *Macromol. Chem. Phys.* **2003**, *204*, 1832−1841.
(57) Nix, W. D.; Gao, H. *J. Mech. Phys. Solids* **1998**, *46*, 411−425.
(58) Shen, L.; Phang, I. Y.; Chen, L.; Liu, T. X.; Zeng, K. Y. *Polymer* **2004**, *45*, 3341−3349.
(59) Shaffer, M. S. P.; Fan, X.; Windle, A. H. *Carbon* **1998**, *36*, 1603−1612.
(60) Ramesh, C.; Bhoje Gowd, E. *Macromolecules* **2001**, *34*, 3308−3313.
(61) Medellin-Rodriguez, F. J.; Larios-Lopez, L.; Zapata-Espinoza, A.; Davalos-Montoya, O.; Phillips, P. J.; Lin, J. S. *Macromolecules* **2004**, *37*, 1799−1809.
(62) Liu, T. X.; Tjiu, W. C.; He, C. B.; Na, S. S.; Chung, T. S. *Polym. Int.* **2004**, *53*, 392−399.
(63) Liu, T. X.; Liu, Z. H.; Ma, K. X.; Shen, L.; Zeng, K. Y.; He, C. B. *Compos. Sci. Technol.* **2003**, *63*, 331−337.
(64) Murthy, N. S. *Polym. Commun.* **1991**, *32*, 301−305.
(65) Lincoln, D. M.; Vaia, R. A.; Wang, Z.-G.; Hsiao, B. S. *Polymer* **2001**, *42*, 1621−1631.
(66) Bonnet, M.; Rogausch, K.-D.; Petermann, J. *Colloid Polym. Sci.* **1999**, *277*, 513−518.
(67) Liu, T. X.; Yan, S. K.; Bonnet, M.; Lieberwirth, I.; Rogausch, K.-D.; Petermann, J. *J. Mater. Sci.* **2000**, *35*, 5047−5055.
(68) Liu, T. X.; Petermann, J. *Polymer* **2001**, *42*, 6453−6461.
(69) Liu, T. X.; Petermann, J.; He, C. B.; Liu, Z. H.; Chung, T.-S. *Macromolecules* **2001**, *34*, 4305−4307.
(70) Liu, T. X. *Eur. Polym. J.* **2003**, *39*, 1311−1317.
(71) Lincoln, D. M.; Vaia, R. A.; Wang, Z.-G.; Hsiao, B. S.; Krishnamoorti, R. *Polymer* **2001**, *42*, 9975−9985.
(72) Medellin-Rodriguez, F. J.; Burger, C.; Hsiao, B. S.; Chu, B.; Vaia, R. A.; Phillips, S. *Polymer* **2001**, *42*, 9015−9023.

MA049132T